J Mater Sci: Mater Electron (2018) 29:1258–1263
DOI 10.1007/s10854-017-8030-z

Nanoindentation creep on Cu_3Sn, Cu_6Sn_5 and $(Cu, Ni)_6Sn_5$ intermetallic compounds grown in electrodeposited multilayered thin film

A. S. M. A. Haseeb[1] · Abu Zayed Mohammad Saliqur Rahman[1,2] · Pay Ying Chia[1]

Received: 15 July 2017 / Accepted: 10 October 2017 / Published online: 23 October 2017

Abstract Tin-based multilayered thin films were fabricated for application in three dimensional microelectronic packaging as joining materials. During device fabrication and application, interconnecting materials can be fully converted to intermetallic compounds (IMCs). As known, IMCs are generally brittle and associated with void formation which can make interconnection in the microelectronic devices vulnerable. In an effort to improve the reliability of the Sn–Cu based IMC, ultra thin layers of Ni (70 nm) were inserted into Cu/Sn system. Electrochemical deposition technique was used to fabricate the samples. Isothermal aging at 150 °C for 168 h was performed to grow the IMCs at required thickness for measuring creep by nanoindentation. Creep strain rate was calculated from experimental data. Creep resistance was significantly improved after adding the small amount of Ni in Cu/Sn multilayered thin film system.

1 Introduction

Tin-based alloys are used in ultra-small interconnections in three-dimensional (3-D) microelectronic packages. During device fabrication and application, the interconnecting materials can be completely converted into Sn–Cu based intermetallic compounds (IMCs) such as Cu_3Sn and Cu_6Sn_5. As known, these IMCs are generally brittle and thus make interconnects vulnerable against thermal stress it experiences during the lifetime of electronic devices. For example, in multilayered interconnects, Kirkendall voids can be found in Cu_3Sn layer or near the interface between Cu_3Sn and plated Cu substrate after aging or during the application time which will strongly impact the reliability of the IMC interconnections [1–3]. Although Cu_6Sn_5 could have better mechanical properties than Cu_3Sn, it could be unstable in thin film system at room temperature [4]. Ni prevents the thermal expansion of Cu_6Sn_5, which could reduce the stress in the interconnects during thermal cycling [5]. Addition of Ni can solve the issue related to phase stability, void and crack formation, which normally observed in case of Cu_6Sn_5 and Cu_3Sn. This eventually leads to better mechanical properties for interconnecting materials. In an effort to modify the interconnecting materials, we report here the effect of the very small amount of Ni addition in the Sn-Cu system. We insert by electrodeposition ultra thin layers of Ni (70 nm) in between Cu and Sn layers which undergo reactive dissolution at the reflow temperature and cause the alloying of IMC.

Electrochemical deposition is a simple, economical and flexible method to deposit various types of thin films [6–8]. Nanoindentation is a non-destructive and highly sophisticated tool to measure mechanical properties of materials at the nanoscale. It has been used to measure mechanical properties in various materials including mechanical metamaterials, biomaterial, electronic and energy materials [9–11]. This technique is also being used to study mechanical and creep properties of lead-free solder based interconnecting materials [12, 13]. In this article, we used nanoindentaion technique to study creep properties of IMCs in electrochemically deposited Cu/Sn and Cu/Ni/Sn systems. At elevated temperature, all the layers of Cu, Sn and Ni reacted and form

✉ A. S. M. A. Haseeb
haseeb@um.edu.my

✉ Abu Zayed Mohammad Saliqur Rahman
zayed@um.edu.my; rahman.168@osu.edu

[1] Department of Mechanical Engineering, University of Malaya, 50603 Kuala Lumpur, Malaysia

[2] Present Address: Department of Mechanical and Aerospace Engineering, Ohio State University, Columbus, OH 43210, USA

IMCs. As joining in advanced microelectrotonics would be evolving towards thin film interconnects, these IMCs will play a very important role in reliability issues of the electronic devices. Thus, it is very important to determine the creep properties of these IMCs. Nogita et al. reported that the mechanical, creep and crack properties of Cu_6Sn_5, $(Cu, Ni)_6Sn_5$ depends on crystal orientation [14]. However, creep properties of IMC layers which have been grown in electrochemically deposited Cu/Sn and Cu/Ni/Sn thin films were not reported till now except in a proceeding of International Electronics Manufacturing Technology Symposium [15]. We studied creep properties of Cu_3Sn, Cu_6Sn_5 and $(Cu, Ni)_6Sn_5$ IMCs after aging by using nanoindentation creep. From experimental data, we estimated creep strain rate and stress exponent for all the IMCs. It shows that addition of trace element of Ni significantly improved the creep properties of lead-free interconnectors.

2 Experimental

Cu/Sn and Cu/Ni/Sn multilayered thin films were prepared by sequential electrodeposition of Cu, Sn and Ni layers using copper pyrophosphate, tin methanesulfonic and nickel Watts baths [16]. A schematic diagram of the synthesized films was given in Fig. 1. Prepared samples were reflowed at 250 °C for 60 s using convection reflow oven (C.I.F FT-02, France). Isothermal aging at 150 °C for 168 h was performed in an oven (Memmert, USA) to develop the phases. Both as-reflowed and aged samples were prepared for cross sectional examination by standard metallographic technique with polishing down to 0.02 μm using silica suspension. FEI Quanta 450 Field-emission Scanning Electron Microscope (FESEM) was used to examine the cross-section at samples. Energy dispersive X-ray spectroscopy (EDX)- Oxford was used to determine the composition of the multilayered system. Fine incident electron beam allows the estimation of composition from a small interaction volume. The phases

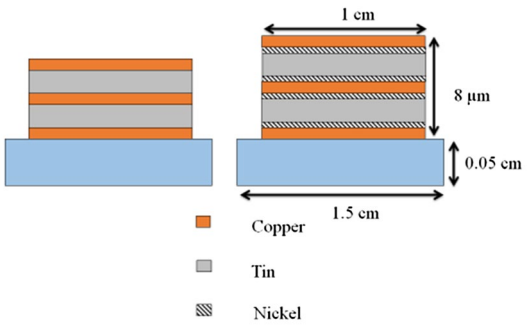

Fig. 1 Schematic of the cross sections of electrodeposited multilayered interconnect showing Cu/Sn/Cu (left) and Cu/Ni/Sn/Cu (right)

of the multilayer sample after long reflow were investigated by X-ray Diffraction using a PanAnalytical diffractometer with Cu Kα radiation which has a wavelength, λ of 0.15418 nm. The step size used was 0.26° and the scan step time was 2.11 s. Peaks shown in the XRD pattern were identified by using the International Centre for Diffraction Data (ICDD) database.

Nanoindentation creep tests were performed in a Hysitron Triboindenter 750 Ubi system at ambient temperature using a Berkovich diamond indenter. Minimum thermal drift rate at < 0.05 nm/s was maintained during the test. Creep tests were performed at a constant load of 4000 μN. The load was initially applied at a loading rate of 400 μN/s. Holding time was 600 s for all the samples. Six to nine measurements were performed on the IMCs formed in Cu/Sn and Cu/Ni/Sn. Care has been taken during creep nanoindentation test to minimize the spacing effects. Average surface roughness was measured to be 27 nm in aged Cu/Ni/Sn whereas 21 nm for aged Cu/Sn sample before nanoindentation. To determine the contact area A of the Berkovich tip, a series of indents at various contact depths were performed on fused quartz and the contact area A was calculated according to the following equation:

$$A = C_0 h_c^2 + C_1 h_c + C_2 h_c^{1/2} + C_3 h_c^{1/4} + C_4 h_c^{1/8} + C_5 h_c^{1/16} \quad (1)$$

where h_c is the contact depth. C_0 for an ideal Berkovich tip is 24.5. C_1 through C_5 should vary in order to fit the shape of the actual probe geometry.

3 Results and discussion

Aging was performed on the reflowed Cu/Sn and Cu/Ni/Sn thin film systems which are shown in Fig 2a and b respectively. As seen in Fig. 2a, the dark gray layer corresponds to Cu_3Sn, while the light gray layer corresponds to Cu_6Sn_5. The EDX analysis is shown in Table 1. It is seen that after subjecting the Cu/Sn sample to 168 h of 150 °C solid state aging, two thick layers of Cu_3Sn separated by a Cu_6Sn_5 IMC layer in the middle grew. The microstructure of the Cu_3Sn IMC is columnar, which is common for Cu_3Sn IMC after aging [17, 18]. With the addition of nickel, it is seen that $(Cu, Ni)_6Sn_5$ IMC (lighter contrast) grew. But the Cu_3Sn IMC layers (IMC with the darker contrast) did not grow after 168 hours of aging (Fig. 2b). These observations are in good agreement with previous literature where the addition of Ni has been forced to suppress Cu_3Sn IMC growth [19, 20]. After aging for 168 hours, average thickness of Cu_3Sn and Cu_6Sn_5 layers becomes 2.35 and 1.7 μm, respectively in Cu/Sn sample. The layer thickness of Cu_3Sn reduced to be 0.5 μm in Cu/Ni/Sn sample. Average thickness of $(Cu, Ni)_6Sn_5$ was measured to be 5 μm.

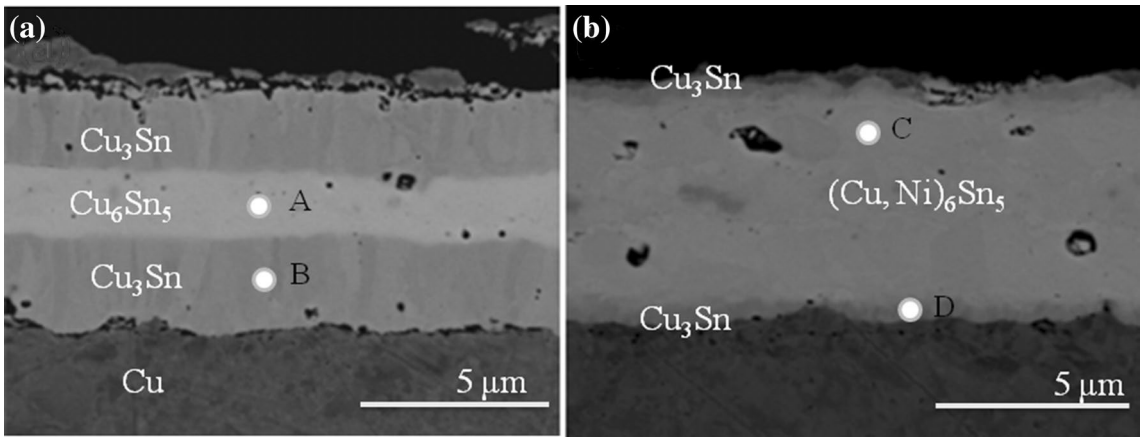

Fig. 2 FESEM micrographs showing cross sectional images of Cu/Sn (**a**) and Cu/Ni/Sn/Cu (**b**) after 168 h of aging at 150 °C

Table 1 EDX analysis of the spots shown in Fig. 2

Spot	Cu	Composition (at.%)		Ratio		Phase identified
		Sn	Ni			
A	57.45	42.55		Cu:Sn	6.75:5.00	Cu_6Sn_5
B	76.68	23.32		Cu:Sn	3.29:1.00	Cu_3Sn
C	51.55	41.76	6.69	Cu+Ni:Sn	6.97:5.00	$(Cu, Ni)_6Sn_5$
D	69.27	30.73		Cu:Sn	2.25:1.00	Cu_3Sn

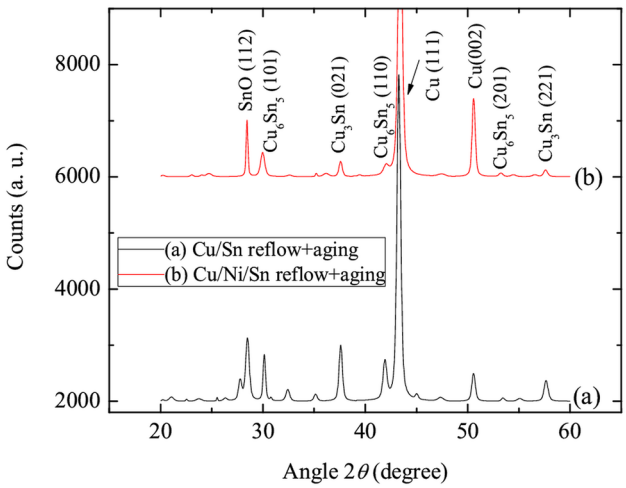

Fig. 3 XRD patterns for Cu/Sn and Cu/Ni/Sn multilayered thin films after reflow at 250 °C following 168 h of aging at 150 °C

Figure 3 shows the XRD patterns for both Cu/Sn and Cu/Ni/Sn system subjected to 168 h of isothermal aging at 150 °C. Strong peak for Cu (ICDD card no. 98-065-5129) came from the substrate as very little amount of yet to dissolve Cu left inside the layers. SnO peaks (ICDD card no. 01-077-2296) indicate that some unreacted Sn gets oxidized during aging at normal atmosphere. After the addition of ultra thin Ni layer (70 nm) in between Cu and Sn layers, similar peaks appeared. The relatively lower intensity of Cu_3Sn peak compared with Cu_6Sn_5 peak which suggests the presence of smaller amount of Cu_3Sn. This is in a good agreement with FESEM images shown in Fig. 2.

Earlier results [16] showed that when Ni nanoparticles were incorporated into the solder, they underwent reactive dissolution, got dissolved in Cu_6Sn_5 IMC and turned it into $(Cu, Ni)_6Sn_5$. In the present case, the 70 nm thick Ni layer underwent reactive dissolution during reflow and aging leading to the formation of $(Cu, Ni)_6Sn_5$. It is known that Ni atoms enter the lattice of Cu_6Sn_5 and replace some of the Cu atoms in the lattice. Table 1 shows that 6.69 at% Ni is dissolved in $(Cu, Ni)_6Sn_5$ in the prepared sample.

Three distinct phases namely Cu_3Sn, Cu_6Sn_5 and $(Cu, Ni)_6Sn_5$ in the reflowed and aged samples were subjected to nanoindentation creep. The Cu_3Sn and Cu_6Sn_5 phases were tested in the Cu/Sn samples (Fig. 2a) and $(Cu, Ni)_6Sn_5$ phase was tested in Cu/Ni/Sn (Fig. 2b) sample. Figure 4 shows the average time-displacement curves for the IMC phases Cu_3Sn (a), Cu_6Sn_5 (b) and $(Cu, Ni)_6Sn_5$ (c). Six to nine indents were taken on the IMCs and averages (d) were calculated based on all the curves. It is seen that upon the application of the load (4000 μN) the displacement increases abruptly. This is termed as instantaneous displacement. The displacement then continues to increase with time as the load is kept constant. This is time-dependent displacement. The values of the instantaneous, time dependent and

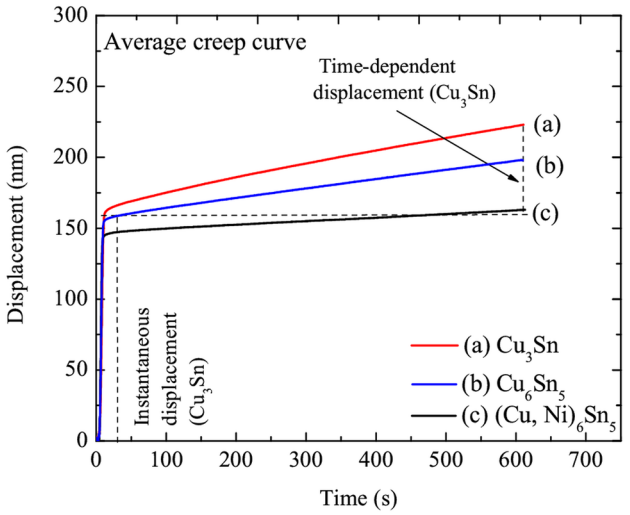

Fig. 4 Average time-displacement curves for three IMCs (*a*) Cu_3Sn, (*b*) Cu_6Sn_5 and (*c*) $(Cu, Ni)_6Sn_5$

total displacement are given in Table 2. It is observed that the instantaneous displacement is the highest for Cu_3Sn (curve a) followed by Cu_6Sn_5 (curve b). $(Cu, Ni)_6Sn_5$ exhibits the lowest instantaneous displacement (curve c). As for the time-dependent displacement, Cu_3Sn displays the highest value. Cu_6Sn_5 has a lower time-dependent displacement, while $(Cu, Ni)_6Sn_5$ shows the lowest values. Thus both instantaneous and time dependent displacement have been reduced when Ni is added. Instantaneous displacement is related to plasticity whereas time dependent displacement is related to creep phenomenon [21]. Table 3 reproduces the hardness values of the three IMCs from an earlier report [4]. A comparison of Tables 2 and 3 shows that IMC with higher hardness exhibits lower instantaneous displacements. Cu_3Sn shows higher displacement value compared with that of Cu_6Sn_5. This is consistent with their hardness.

Figure 5 shows the creep strain rate for Cu_3Sn (a), Cu_6Sn_5 (b) and $(Cu, Ni)_6Sn_5$ estimated from following equation [22]:

$$\dot{\varepsilon} = \dot{h}/h \tag{2}$$

where $\dot{h}$ is indentation displacement rate (dh/dt) and h is instantaneous displacement.

Steady state creep strain rate values for Cu_3Sn, Cu_6Sn_5 and $(Cu, Ni)_6Sn_5$ are furnished in Table 2. It can be seen

Table 3 Hardness of three IMCs [4]

IMCs	Hardness
Cu_3Sn	5.99 ± 0.39
Cu_6Sn_5	6.61 ± 0.25
$(Cu, Ni)_6Sn_5$	7.43 ± 0.57

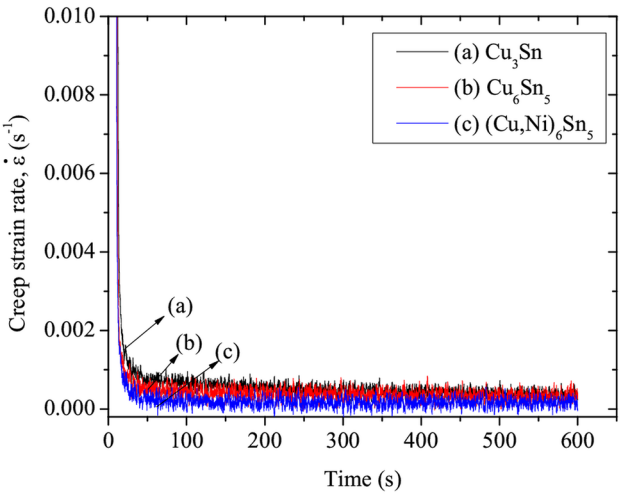

Fig. 5 Creep strain rate calculated from Eq. 1 for all three IMCs

that after the addition of Ni, the steady state creep strain rate reduced significantly. Thus the incorporation of Ni has lead to the improvement of creep resistance. Improvement of creep properties in IMC was also observed by addition of Ni in bulk system [14]. Mechanism behind the improvement of creep properties after addition of very small amount of Ni is not fully understood.

Creep stress exponent, n has been estimated from the following relationship between creep strain rate, $\dot{\varepsilon}$ and stress, σ (P/A) :[23]

$$\dot{\varepsilon} = k.\sigma^n \tag{3}$$

Equation 2 can be written as below by taking log on both side:

$$Log\left(\frac{1}{h}.\frac{dh}{dt}\right) = Logk + n.Log\left(\frac{P_{const}}{A}\right) \tag{4}$$

Table 2 Instantaneous, total, time-dependent displacement and steady state strain rate of three IMCs with creep stress exponent

IMCs	Instantaneous displacement (nm)	Time-dependent displacement (nm)	Total displacement (nm)	Steady state Strain rate ($\times 10^{-4}$ s^{-1})
Cu_3Sn	161 ± 8	62 ± 16	223 ± 17	4.6
Cu_6Sn_5	154 ± 6	41 ± 15	198 ± 12	3.7
$(Cu, Ni)_6Sn_5$	144 ± 4	19 ± 7	163 ± 5	1.9

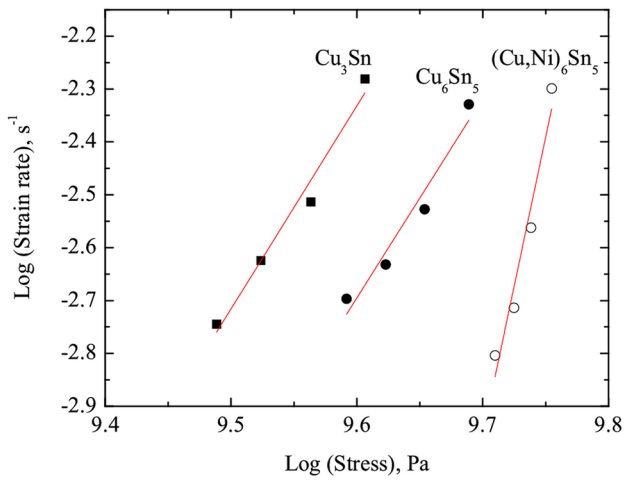

Fig. 6 Creep stress exponent, n value was calculated from the linear curve fitting of the log of strain rate and stress for three IMCs

Table 4 Creep stress exponent values for three intermetallics Cu_3Sn, Cu_6Sn_5 and $(Cu,Ni)_6Sn_5$

IMCs	Experimental parameters Constant load (μN), holding time (s)	Creep exponent value, n	References
Cu_3Sn	4000, 600	4.8	This work
	5000, 200	21.7	[26]
Cu_6Sn_5	4000, 600	4.8	This work
	5000, 200	37.3	[26]
	2000, 60	34.9	[27]
$(Cu, Ni)_6Sn_5$	4000, 600	11.3	This work
	2000, 60	43.1	[27]

where k is a constant, P is the applied constant load and A is projected contact area of a Berkovich tip. Creep stress exponent can be obtained by linear regression fitting of Eq. 3 (Fig. 6) which is given in Table 4. n values of Cu_3Sn and Cu_6Sn_5 are found to be 4.8 whereas that of $(Cu, Ni)_6Sn_5$ is 11.3. Usually n value lies between 4–7 for most pure metal and metallic alloys [24] which means creep is governed by dislocation glide or climb (power-law creep) and is grain-size independent [25]. Since the n value of both Cu_3Sn and Cu_6Sn_5 is close to 5, dislocation creep is the dominant mechanism. After the addition of Ni in Cu/Sn system, the n increased to 11.3 which suggests that the creep resistance has increased due to the addition of Ni.

Table 4 shows the values of n of different IMC phases obtained by researchers. It is seen that n values obtained in this work are much lower compared with those obtained by others. The reason for this discrepancy is not clear. It could be related to the different processing as well as creep test conditions used in this study.

According to deformation mechanism maps [28], creep at low temperature is dominated by plasticity where dislocation glide is the dominant mechanism. Dislocation glide is a thermally activated process. The mechanism of dislocation glide depends on the crystal structure. For fcc metals, dislocation glide is controlled by discrete obstacles. For other crystal structures, lattice resistance may play the dominant role. This is because the lattice resistance of fcc crystals is two to three order of magnitude lower than that of non fcc crystals [29]. In the present IMCs e.g., Cu_6Sn_5/$(Cu,Ni)_6Sn_5$ with monoclinic structure, dislocation motion controlled by lattice resistance is likely to be the dominant mechanism. It is suggested that the incorporation of Ni in the IMC lattice has increased the lattice resistance. Solid solution effect is also expected to play a role. The segregation of solute atoms to grain boundary can also lead to creep retardation [30].

For dislocation glide controlled by lattice resistance, the strain rate depends on different factor as follows [28]:

$$\dot{\epsilon} \propto \exp - \left\{ \frac{\Delta F}{kT} \left[1 - \left(\frac{\sigma_s}{\hat{\tau}} \right)^{3/4} \right]^{4/3} \right\} \tag{5}$$

where,

$\dot{\epsilon}$ = Strain rate
ΔF = Helmotz free energy of an isolated pair of dislocation kinks
σ_s = Applied stress
$\hat{\tau}$= Athermal flow strength or flow stress at 0 K
k= Boltzman constant
T = Creep test temperature in K

It was shown [31] that the instantaneous displacement in an indentation creep test is mainly determined by the athermal flow strength, $\hat{\tau}$, while the time dependent displacement is mainly influenced by the energy term, ΔF. In the present case, the incorporation of Ni reduced both the instantaneous displacement and time dependent displacement. Thus, the presence of Ni in the IMC lattice is likely to increase both the athermal flow strength and the energy term. Further investigations are necessary in this direction.

4 Summary

We have conducted creep experiments by using nanoindentaion on three intermetallics Cu_3Sn, Cu_6Sn_5 and $(Cu,Ni)_6Sn_5$ prepared by electrodeposition, reflow and isothermal aging. IMCs were confirmed by XRD and EDX. From the value of creep stress exponent n, it can be said that creep resistance increased significantly when Ni is introduced into the Cu/Sn system by in situ dissolution of electrodeposited Ni

nanolayer during reflow. This would eventually increase the reliability of interconnecting materials in advanced electronic devices.

Acknowledgements Authors would like to acknowledge High Impact Research grant, University of Malaya from Ministry of Higher Education, Malaysia (Project No. UM.C/625 /1/HIR/ MOHE/ENG/26).

References

1. L. Mo, Z. Chen, F. Wu, C. Liu, Intermetallics **66**, 13 (2015)
2. K. Zeng, R. Stierman, T.C. Chiu, D. Edwards, K. Ano, K.N. Tu, J. Appl. Phys. **97**, 024508 (2005)
3. D. Kim, J.H. Chang, J. Park, J.J. Pak, J. Mater. Sci. **22**, 703 (2011)
4. A.Z.M.S. Rahman, P.Y. Chia, A.S.M.A. Haseeb, Mater. Lett. **147**, 50 (2015)
5. D. Mu, J. Read, Y. Yang, K. Nogita, J. Mater. Res. **26**, 2660 (2011)
6. Y. Zhao, P. Moreau, M.R. Plouet, J.L. Duvail, Electrochim. Acta **151**, 347 (2015)
7. Z. Lu, M. Sun, T. Xu, Y. Li, W. Xu, Z. Chang, Y. Ding, X. Sun, L. Jiang, Adv. Mater. **27**, 2361 (2015)
8. C.I. Cuello, C. Broussillou, V. Bermudez, E. Saucedo, A. Perez-Rodriguez, V.I. Roca, Appl. Phys. Lett. **105**, 021905 (2014)
9. X. Zheng, H. Lee, T.H. Weisgraber, M. Shusteff, J. Deotte, E.B. Duoss, J.D. Kuntz, M.M. Biener, Q. Ge, J.A. Jackson, S.O. Kucheyev, N.X. Fang, C.M. Spadaccini, Science **344**, 1373 (2014)
10. H.D. Espinosa, R.A. Bernal, M.M. Jolandan, Adv. Mater. **24**, 4656 (2012)
11. L. Li, C. Ortiz, Nat. Mater. **13**, 501 (2014)
12. V.M.F. Marques, B. Wunderle, C. Johnston, P.S. Grant, Acta Mater. **61**, 2471 (2013)
13. L. Jiang, N. Chawla, Scripta Mater. **63**, 480 (2010)
14. D. Mu, H. Huang, S.D. McDonald, J. Read, K. Nogita, Mater. Sci. Eng. A **566**, 126 (2013)
15. A. Z. M. S. Rahman, P. Y. Chia, A. S. M. A. Haseeb, Proceedings of the IEEE/CPMT International Electronics Manufacturing Technology Symposium, Article number: 7123130 (2015)
16. P.Y. Chia, A.S.M.A. Haseeb, J. Mater. Sci. **26**, 294 (2015)
17. J.F. Li, P.A. Agyakwa, C.M. Johnson, Acta Mater. **59**, 1198 (2011)
18. M.S. Park, S.L. Gibbons, R. Arroyave, Acta Mater. **60**, 6278 (2012)
19. S.L. Tay, A.S.M.A. Haseeb, M.R. Johan, P.R. Munroe, M.Z. Quadir, Intermetallics **33**, 8 (2013)
20. Y.W. Wang, C.C. Chang, C.R. Kao, J. Alloys Compd. **478**, L1–L4 (2009)
21. A.C. Fischer-Cripps, Mater. Sci. Eng. A **385**, 74 (2004)
22. L. Shen, P. Lu, S. Wang, Z. Chen, J. Alloys Compd. **574**, 98 (2013)
23. Y.C. Liu, J.W.R. Teo, S.K. Tung, K.H. Lam, J Alloys Compd. **448**, 340 (2008)
24. M.E. Kassner, M.T. Prez-Prado, *Fundamentals of Creep in Metals and Alloys* (Elsevier, Oxford, 2009)
25. I.C. Choi, B.G. Yoo, Y.A. Kim, J. Jang, J. Mater. Res. **27**, 3 (2012)
26. J.M. Song, C.W. Su, Y.S. Lai, Y.T. Chiu, J. Mater. Res. **25**, 629 (2010)
27. D. Mu, H. Huang, S.D. Mcdonald, K. Nogita, J. Electron. Mater. **42**, 304 (2013)
28. H.J. Frost, M.F. Ashby, *Deformation-Mechanism Maps: The Plasticity and Creep of Metals and Ceramic* (Pergamon Press, Oxford, 1982)
29. Y. Kamimura, K. Edagawa, S. Takeuchi, Acta Mater. **61**, 294 (2013)
30. J. Cho, C.M. Wang, H.M. Chan, J.M. Rickman, M.P. Harmer, Acta Mater. **47**, 4197 (1999)
31. A.S.M.A. Haseeb, Comput. Mater. Sci. **37**, 278 (2006)